Journal of Sound and Vibration (2002) **253**(5), 1015–1037
doi:10.1006/jsvi.2001.4048, available online at http://www.idealibrary.com on IDEAL®

HIGHER VIBRATION MODES IN RAILWAY TRACKS AT THEIR CUT-OFF FREQUENCIES

M. R. Pfaffinger and J. Dual

Institute of Mechanical Systems, ETH Zentrum, 8092 Zurich, Switzerland.
E-mail: juerg.dual@imes.mavt.ethz.ch

(*Received* 18 *December* 2000, *and in final form* 14 *September* 2001)

Forced vibrations of a railway track excited at the cut-off frequency of one of its wave modes are examined theoretically, numerically and experimentally in the frequency range from 5 to 50 kHz. The background of this paper is the new idea of using the local vibration zone of the rail close to the excitation to detect passing train wheels. An important parameter which influences this local vibration zone is system damping. The determination of a new quality factor to characterize damping of a system which both resonates and interacts with travelling waves is first studied in the case of a beam on a viscoelastic foundation. Some key differences compared with a single-degree-of-freedom (s.d.o.f.) mechanical oscillator are pointed out and an adopted damping measurement method is suggested. The phenomenological behavior of higher vibration modes is then investigated using a model of several elastically connected beams referred to as the multiple-mode model. Modal damping is introduced and the model is studied both in a continuous and in a discretely supported configuration. Both localized and non-localized modes are observed in the latter case. The cut-off frequencies and mode shapes are also determined experimentally at a real test track using a scanning laser interferometer and show good agreement with numerical calculations. The spatial behavior of the measured system response at the test track corresponds well to the effects predicted by the multiple-mode model. Damping measurements are performed and the quality factors of several modes are determined and discussed.

1. INTRODUCTION

This paper examines the forced vibration response of a railway track excited at the cut-off frequency of one of its wave modes. At these frequencies, a local vibration zone builds up close to the excitation in the presence of damping. Often these frequencies are also called transverse resonance frequencies. The background of this study is the idea to develop a sensor which detects train axles by measuring the interaction between passing train wheels and this local vibration. Devices for detecting the presence of railroad cars are called rail contacts and are used, e.g., for mobile warning systems to be employed at railway construction sites to guarantee the safety of working staff. Today's most often used rail contacts are mechanical or optical switches or inductive sensors. All of these devices are sensitive to certain interferences such as pollution or magnetic fields, thus leaving a strong industrial need for improvements.

The power spectrum of mechanical vibrations of the rail caused by passing trains shows large signal amplitudes mainly below approximately 10–15 kHz. This implies that the signal-to-noise ratio of a sensor which is based on forced rail vibrations can be improved by using frequencies above 15 kHz. However, as the density of cut-off frequencies increases

0022-460X/02/$35.00

towards higher frequencies and as the mode shapes of the cross-sectional rail deformation become more and more complicated, a technique must be developed which allows the sensor to find vibration modes suitable for wheel detection.

Vibration modes are suitable for wheel detection if several conditions are met. First of all, a local vibration zone must exist. For a strong interaction, the corresponding mode shape must show a large vibration amplitude at the contact point between the wheel and the rail. It is also required that the mode shape has no nodes at the running surface along which a wheel could travel without being detected. Furthermore, the mechanical reaction time of the vibration mode must be fast enough to detect wheels of fast travelling trains.

This paper focuses on the forced vibration behavior of higher modes in railway tracks at their cut-off frequencies. The frequency range of this study is set to 5–50 kHz. The goal of the study is to identify the parameters influencing the cut-off frequency behavior. This knowledge is necessary in order to develop a sensor which is capable of reliably finding suitable railmodes.

At frequencies above approximately 1500 Hz, the cross-section of the rail deforms significantly and the rail has its first cut-off frequencies. Various concepts which take this into account in regard to dynamic track modelling are found in the literature. The development of mathematical track models is mostly motivated by the need to understand and perhaps even solve practical problems arising from dynamic loads such as corrugation of wheel and rail, noise and ground-borne vibration. Ripke and Knothe [1] used two Timoshenko beams representing the head and the foot of the rail with an elastic coupling in between. Scholl [2] calculated the dispersion relations of 11 wave modes up to a frequency of 15 kHz by modelling the head, the web and the foot of the rail by plates of constant thickness. Thompson [3] modelled a 10 m long section of the rail including sleepers, rail pads and ballast as equivalent continuous layers of mass and stiffness with finite elements, and then applied periodic structure theory to calculate the response of the infinite system. Strzyzakowski and Ziemanski [4] introduced an FEM cross-sectional solution together with an analytical treatment in the longitudinal direction. Knothe *et al.* [5] compared models of rails as published by Grassie *et al.* [6], Ripke and Knothe [1], Scholl [2] and Strzyzakowski and Ziemanski [4] in the frequency range up to 15 kHz and thus established the validity ranges of these models. The frequency limit of 15 kHz is considered to be sufficient for the practical problems involving rails, as it represents the limit of human hearing. Track models developed for these high frequencies are commonly based on the assumption of a continuous structure, thus ignoring the discrete support on sleepers. Damping effects are usually neither included nor discussed. No previously published study has been found which suggests that advantage be taken of rail vibrations for a technical application as in the proposed wheel detection concept.

The most important parameters regarding the dynamic response of the rail for this application are the geometry and material properties of the cross-section, the system damping and the parameters of the supports. These parameters include the stiffness of the support which depends on the type of pads and sleepers (i.e., wooden or concrete sleepers), on ballast parameters, and on the geometry of the support (e.g., sleeper spacing).

The upper frequency limit of 50 kHz aimed at within this study is considerably higher than the frequency range covered by present track models. The development of a detailed finite element model of the situation which has been examined would entail great expense both regarding modelling and computational effort while hiding the respective influences of the model parameters. Therefore, a different approach is chosen in this study. In section 2, the forced vibration response of a waveguide close to its cut-off frequencies is studied using analytical models. The section begins with a discussion of the damping characterization of

a Bernoulli–Euler beam on a viscoelastic support. Higher vibration modes are then included by studying a model of several elastically connected beams. The solution is derived in a way which allows the implementation of modal damping. The model is studied in both a continuously and a discretely supported configuration. This model is later referred to as the multiple-mode model. Ripke and Knothe [1] and, more recently, Wu and Thompson [7, 8] used similar models with two Timoshenko beams representing the head and the foot of the rail which are elastically connected. However, the elements of the multiple-mode model suggested here should not be viewed as a valid representation of physical track components. The multiple-mode model serves merely as a vehicle to qualitatively study the effects of higher vibration modes at their cut-off frequency as well as effects of discrete supports.

Based on the knowledge gained from the multiple-mode model, the cut-off frequencies and mode shapes can be numerically predicted for a real track in an efficient way. This is shown in section 3 with reference to the corresponding literature.

The statements about the forced vibration behavior derived in the theoretical and numerical part of this paper are then experimentally verified by measurements performed at a test track. The results of these measurements are presented and discussed in section 4.

The investigation of the interaction between passing train wheels and the local vibration is outside the scope of this paper. The applicability of the proposed wheel detection method has been studied by Pfaffinger [9].

2. THEORETICAL CONSIDERATIONS

2.1. Q^{BW}-FACTOR OF A BEAM ON VISCOELASTIC FOUNDATION

Figure 1 shows a purely elastic Bernoulli–Euler beam on a continuous viscoelastic foundation excited by a harmonic point force $\hat{p}(z = 0, t) = p e^{i\omega t}$ with angular frequency ω. The differential equation of this model in the case of harmonic motion is

$$EIu_{,zzzz} - \omega^2 \rho A u + i\omega c_c u + s_c(1 + i\eta)u = 0, \tag{1}$$

where $u = u(z, t)$ is the downward displacement, and subscripts after the comma denote partial differentiation with respect to the designated variable. In equation (1) EI, ρ and A are the flexural stiffness, the mass per unit volume and the cross-sectional area of the beam, respectively. The support has the stiffness s_c and the viscous damping constant c_c per unit length. In addition to viscous damping, hysteretic damping η is introduced by adding a complex component $i\eta s_c$ to the support stiffness.

By defining dimensionless time and space variables $\tau = \omega_1 t$ and $\zeta = \gamma z$, equation (1) may be put in the dimensionless form

$$w_{,\zeta\zeta\zeta\zeta} - \kappa^2 w + 2i\kappa\delta w + i\eta w + w = 0, \tag{2}$$

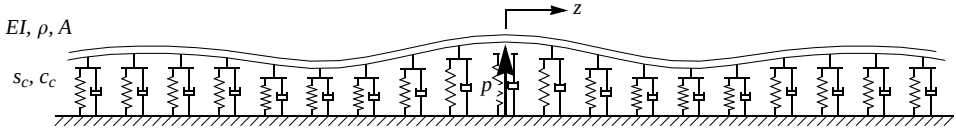

Figure 1. Bernoulli–Euler beam on a continuous viscoelastic foundation with excitation force at $z = 0$ m.

where $\omega_1 = \sqrt{s_c/\rho A}$, $\gamma = \sqrt[4]{s_c/EI}$, $\delta = c_c/\sqrt{4 s_c \rho A}$, $w = (EI\gamma^3/p)u$ and $\kappa = \omega/\omega_1$. Considering steady-state solutions of the form

$$w(\zeta, \tau) = b e^{i(\alpha\zeta + \kappa\tau)}, \tag{3}$$

equation (2) is solved if the dimensionless wavenumber α satisfies the condition $\alpha^4 = \kappa^2 - 1 - i(2\delta\kappa + \eta)$ giving four branches of the wavenumber.

Taking into account the radiation condition for $\zeta \to \infty$ and the boundary conditions at $\zeta = 0$ gives the forced vibration solution (4) for $\zeta \geqslant 0$ of an infinite beam on a continuous viscoelastic support,

$$w(\zeta, \tau) = -\tfrac{1}{4}\alpha^{-3}(i e^{-i\alpha\zeta} + e^{-\alpha\zeta}) e^{i\kappa\tau}. \tag{4}$$

The wavenumber is set to $\alpha = \sqrt[4]{|\alpha^4|} e^{i \arg(\alpha^4)/4}$ in equation (4) using the absolute value $|\alpha^4|$ and the argument $\arg(\alpha^4)$ of α^4.

The complex ratio of the displacement at the point of excitation to the exciting force is called the direct receptance. The receptance of the studied system can be written as

$$\beta_c = \sqrt{2}/4 |\alpha|^{-3} e^{-i((3\pi/4) + 3\arg(\alpha))}. \tag{5}$$

At the minimum of $|\alpha|$, the direct receptance reaches its maximum and only system damping prevents the amplitude from increasing to infinity. In the case of small damping parameters δ and η, the first approximation of the frequency, where the direct receptance is maximal, is $\kappa = 1$ corresponding to $\omega = \omega_1$. The frequency ω_1 is called cut-off frequency. In the absence of damping, the entire system performs a synchronous motion and the amplitude tends towards infinity if excited at the cut-off frequency ω_1.

The damping of a classical single-degree-of-freedom (s.d.o.f.) mechanical oscillator is commonly characterized by the quality factor or Q-factor. One method to determine the Q-factor of a s.d.o.f. system is to calculate $Q = 1/(\kappa_2 - \kappa_1)$ where κ_1 and κ_2 are the two dimensionless frequencies above and below the resonance frequency $\kappa = 1$, for which the amplitude of the oscillation has dropped to $1/\sqrt{2}$ of its resonance value respectively. At κ_1 and κ_2 the phase of the transfer function has shifted $\pm \pi/4$ compared with the phase at the resonance frequency. The overall phase change of a classical s.d.o.f. mechanical oscillator is π.

In the case of a Bernoulli–Euler beam on a viscoelastic foundation, the total phase shift of the receptance is $3\pi/4$. This difference compared with an s.d.o.f. oscillator indicates that the concept of the Q-factor cannot be applied directly to characterize the damping behavior of a system which includes wave propagation and which leads to a more appropriate definition to be used in the case considered here.

At the cut-off frequency $\kappa = 1$, the magnitude and phase of the receptance give

$$|\beta_c|_{\kappa=1} = \tfrac{1}{8}(2\delta + \eta)^{3/4} \quad \text{and} \quad \arg(\beta_c)|_{\kappa=1} = -3\pi/4 + 3\pi/8. \tag{6}$$

Motivated by the s.d.o.f. oscillator analysis consider now the receptance at the frequencies κ_a and κ_b which satisfy the conditions

$$\kappa_a^2 - 1 + (2\delta\kappa_a + \eta) = 0 \quad \text{and} \quad \kappa_b^2 - 1 - (2\delta\kappa_b + \eta) = 0. \tag{7}$$

Taking into account the fact that the frequencies must be positive and in the case of small damping parameters δ and η, the first order approximations of the frequencies κ_a and κ_b are

$$\kappa_a = 1 - \delta - \eta/2 \quad \text{and} \quad \kappa_b = 1 + \delta + \eta/2. \tag{8}$$

Adding and subtracting $\pm(2\delta\kappa_{a,b}+\eta)\mp(2\delta\kappa_{a,b}+\eta)$ to the solution of the wavenumber gives

$$\alpha(\kappa_{a,b}) = \sqrt[4]{\kappa_{a,b}^2 - 1 \pm (2\delta\kappa_{a,b}+\eta) \mp (2\delta\kappa_{a,b}+\eta) - \mathrm{i}(2\delta\kappa_{a,b}+\eta)}. \tag{9}$$

By using relations (7) the wavenumber at the frequencies κ_a and κ_b can be rewritten as

$$\alpha(\kappa_{a,b}) = \sqrt[4]{-(2\delta\kappa_{a,b}+\eta)(\mathrm{i}\pm 1)} = \sqrt[8]{2}\,\sqrt[4]{(2\delta\kappa_{a,b}+\eta)}\,\mathrm{e}^{-\mathrm{i}(\pi/8 \pm \pi/16)} \tag{10}$$

giving amplitude and phase values of the receptance function as

$$|\beta_c|_{\kappa_{a,b}} = (1/\sqrt[8]{8})\,\tfrac{1}{8}(2\delta\kappa_{a,b}+\eta)^{-3/4} \quad \text{and} \quad \arg(\beta_c)|_{\kappa_{a,b}} = -3\pi/4 + 3\pi/8 \pm 3\pi/16. \tag{11}$$

By ignoring parts of the order δ^2 and $\delta\eta$, one can see from equations (11) that the magnitude has dropped to $1/\sqrt[8]{8}$ and the phase has shifted $\pm 3\pi/16$ at the frequencies κ_a and κ_b compared with the values at the cut-off frequency. Let one define the ratio between the cut-off frequency and $(\kappa_b - \kappa_a)$ as the Q^{BW}-factor of the continuously supported Bernoulli–Euler beam. The index stands for bending wave. The Q^{BW}-factor is related to the system damping according to the following equation:

$$Q^{BW} = 1/(\kappa_b - \kappa_a) = 1/(2\delta + \eta). \tag{12}$$

With this definition of the Q^{BW}-factor, the relation between the obtained quality factor and the damping parameters of the system is analogous to the corresponding Q-factor definition of a s.d.o.f. mechanical oscillator.

It can be shown by solving the free vibration response of the system that the time constant $t_{1/e}$, after which the amplitude of the vibration has decayed to e^{-1} of its initial value, is related to the Q^{BW}-factor according to equation (13). Again, this is analogous to the corresponding relation in the case of an s.d.o.f. mechanical oscillator,

$$t_{1/e} = 2Q^{BW}/\omega_1. \tag{13}$$

2.2. HIGHER MODE BEHAVIOR

2.2.1. *Model introduction and modal solution*

The next step is to extend the model studied in the previous section to include higher vibration modes. Consider a system of multiple Bernoulli–Euler beams interconnected by elastic layers. Figure 2 shows a schematic of such a model consisting of $n = 3$ beams.

As already pointed out in the introduction, the elements of this model should not be viewed as a valid representation of physical track components. The model is used to get an understanding of the observed phenomenon of forced vibrations at the cut-off frequencies of a waveguide. Many features observed in the experimental investigations presented and discussed in section 4 can be explained using this simple model. Since only the behavior close to the cut-off frequencies, which implies large wavelengths, is of interest in this study, Bernoulli–Euler beams are used instead of Timoshenko beams. This assumption is justified in greater detail later in this section.

The dynamic behavior of the model shown in Figure 2 is described by the set of differential equations (14), where $u_i = u_i(z, t)$ are the absolute downward displacements of

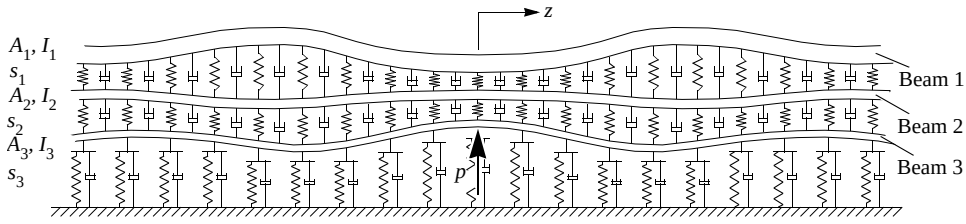

Figure 2. Continuous multiple-mode model consisting of $n = 3$ Bernoulli–Euler beams interconnected by elastic layers.

the three beams:

$$\begin{bmatrix} EI_1 & 0 & 0 \\ 0 & EI_2 & 0 \\ 0 & 0 & EI_3 \end{bmatrix} \begin{bmatrix} u_1 \\ u_2 \\ u_3 \end{bmatrix}_{,zzzz} + \begin{bmatrix} \rho A_1 & 0 & 0 \\ 0 & \rho A_2 & 0 \\ 0 & 0 & \rho A_3 \end{bmatrix} \begin{bmatrix} u_1 \\ u_2 \\ u_3 \end{bmatrix}_{,tt} + \begin{bmatrix} s_1 & -s_1 & 0 \\ -s_1 & s_1 + s_2 & -s_2 \\ 0 & -s_2 & s_2 + s_3 \end{bmatrix} \begin{bmatrix} u_1 \\ u_2 \\ u_3 \end{bmatrix} = 0. \tag{14}$$

No damping is included in equation (14) yet in favor of modal damping, which will be introduced at a later stage.

The set of equations (14) can be written in matrix notation as (15)

$$\mathbf{B}\mathbf{u}_{,zzzz} + \mathbf{M}\mathbf{u}_{,tt} + \mathbf{K}\mathbf{u} = 0, \tag{15}$$

where $\mathbf{u}$ is the displacement vector of the beams and $\mathbf{K}$, $\mathbf{M}$ and $\mathbf{B}$ are the stiffness coefficient matrix of the elastic connections, the mass matrix and the flexural stiffness coefficient matrix of the beams. The final solution of the damped system will be derived stepwise from several subproblems.

Considering the subproblem

$$\mathbf{M}\mathbf{u}_{,tt} + \mathbf{K}\mathbf{u} = 0, \tag{16}$$

corresponding to the free vibration problem of the model cross-section and introducing $\mathbf{u} = \mathbf{b}e^{i\omega t}$ leads to an eigenvalue problem with eigenvalues $\tilde{\omega}_i^2$ and eigenvectors $\tilde{\boldsymbol{\xi}}_i$.

Assembling the eigenvectors according to equation (17) gives the modal matrix $\tilde{\mathbf{E}}_\omega$ which is scaled to meet the conditions (18):

$$\tilde{\mathbf{E}}_\omega = [\tilde{\boldsymbol{\xi}}_1, \ldots, \tilde{\boldsymbol{\xi}}_n], \tag{17}$$

$$\tilde{\mathbf{E}}_\omega^{\mathrm{T}}\mathbf{K}\tilde{\mathbf{E}}_\omega = \mathrm{diag}[\tilde{\omega}_1^2, \ldots, \tilde{\omega}_n^2] = \boldsymbol{\Omega}^2 \quad \text{and} \quad \tilde{\mathbf{E}}_\omega^{\mathrm{T}}\mathbf{M}\tilde{\mathbf{E}}_\omega = \mathbf{I}. \tag{18}$$

The modal matrix $\tilde{\mathbf{E}}_\omega$ is now used to transform the set of differential equations (15), giving

$$\tilde{\mathbf{E}}_\omega^{\mathrm{T}}\mathbf{B}\tilde{\mathbf{E}}_\omega u_{\omega,zzzz} + \mathbf{I}\mathbf{u}_{\omega,tt} + \boldsymbol{\Omega}^2\mathbf{u}_\omega = 0, \tag{19}$$

which can be solved considering steady state solutions $\mathbf{u}_\omega$ of the form

$$\mathbf{u}_\omega = \mathbf{b}_\omega e^{i(\tilde{k}(\omega)z + \omega t)}, \tag{20}$$

where $\tilde{k}(\omega)$ is the wavenumber of the undamped system. Introducing equation (20) into equation (19) yields an eigenvalue problem with eigenvalues $\tilde{k}_i(\omega)^4$ and eigenvectors $\tilde{\boldsymbol{\xi}}_{ki}(\omega)$.

If the frequency is equal to one of the frequencies $\tilde{\omega}_i$ calculated above, the rank of the matrix $(-\omega^2\mathbf{I} + \boldsymbol{\Omega}^2)$ is reduced by one, implying that one of the eigenvalues $\tilde{k}_i(\omega)$ is zero and the corresponding eigenvector $\tilde{\boldsymbol{\xi}}_{ki}(\omega)$ equals $\tilde{\boldsymbol{\xi}}_i$. This means that the frequencies $\tilde{\omega}_i$ calculated from the free vibration problem of the cross-section [equation (16)] are the cut-off frequencies of the system and the vectors $\tilde{\boldsymbol{\xi}}_i$ are the mode shapes of the respective modes at those frequencies in analogy to the s.d.o.f. case.

Similarly, the eigenvectors $\tilde{\boldsymbol{\xi}}_{ki}(\omega)$ are assembled into the frequency-dependent modal matrix

$$\tilde{\mathbf{E}}_k(\omega) = [\tilde{\boldsymbol{\xi}}_{k1}(\omega), \ldots, \boldsymbol{\xi}_{kn}(\omega)] \tag{21}$$

where

$$\tilde{\mathbf{E}}_k^{\mathrm{T}}(\omega)(\boldsymbol{\Omega}^2 - \omega^2\mathbf{I})\tilde{\mathbf{E}}_k(\omega) = \mathrm{diag}[-\tilde{k}_1(\omega)^4, \ldots, -\tilde{k}_n(\omega)^4],$$

$$\text{and} \quad \tilde{\mathbf{E}}_k^{\mathrm{T}}(\omega)\tilde{\mathbf{E}}_\omega^{\mathrm{T}}\mathbf{B}\tilde{\mathbf{E}}_\omega\tilde{\mathbf{E}}_k(\omega) = \mathbf{I}. \tag{22}$$

By applying the modal matrices $\tilde{\mathbf{E}}_\omega$ and $\tilde{\mathbf{E}}_k(\omega)$, the original set of differential equations can be frequencywise decoupled, giving

$$\tilde{\mathbf{E}}_k^{\mathrm{T}}(\omega)\tilde{\mathbf{E}}_\omega^{\mathrm{T}}\mathbf{B}\tilde{\mathbf{E}}_\omega\tilde{\mathbf{E}}_k(\omega)\mathbf{u}_{k,zzzz} + \tilde{\mathbf{E}}_k^{\mathrm{T}}(\omega)\tilde{\mathbf{E}}_k(\omega)\mathbf{u}_{k,tt} + \tilde{\mathbf{E}}_k^{\mathrm{T}}(\omega)\boldsymbol{\Omega}^2\tilde{\mathbf{E}}_k(\omega)\mathbf{u}_k = 0, \tag{23}$$

which can be solved by introducing solutions of the form $\mathbf{u}_k = \mathbf{b}_k e^{\mathrm{i}(k(\omega)z + \omega t)}$. Within the experimental investigation presented in section 4, the damping values of several modes are measured at their cut-off frequencies. The resulting quality factors are interpreted as damping measures assigned to these modes. Motivated by this experimental consideration, both hysteretic and viscous modal damping are introduced to the system at this stage as shown below:

$$(k(\omega)^4\mathbf{I} + \tilde{\mathbf{E}}_k^{\mathrm{T}}(\omega)(\boldsymbol{\Omega}^2 - \omega^2\mathbf{I})\tilde{\mathbf{E}}_k(\omega)$$

$$+ \mathrm{i}\omega\,\mathrm{diag}\,[2(|\tilde{k}_i(0)^4|/(\tilde{\omega}_i)\,\delta_i] + \mathrm{i}\,\mathrm{diag}[\tilde{k}_i(0)^4|\eta_i])\mathbf{b}_k = 0. \tag{24}$$

The undamped wavenumbers $\tilde{k}_i$ at $\omega = 0$ and the cut-off frequencies $\tilde{\omega}_i$ of each mode are used to scale the damping matrices in order to use the same order of magnitude for the damping parameters as in the previously studied case of the continuously supported Bernoulli–Euler beam.

Solutions of the complex equation system (24) exist for the eigenvalues $k_i(\omega)^4$. The corresponding eigenvectors $\boldsymbol{\xi}_{ki}(\omega)$ are again assembled into the frequency-dependent modal matrix

$$\mathbf{E}_k(\omega) = [\boldsymbol{\xi}_{k1}(\omega), \ldots, \boldsymbol{\xi}_{kn}(\omega)]. \tag{25}$$

Please note that the modal matrix $\mathbf{E}_k(\omega)$ has been obtained after introducing modal damping to the system, whereas $\tilde{\mathbf{E}}_k(\omega)$ has been derived in the undamped case.

The final solution of the set of differential equations (15) including damping can be expressed by its modal components as

$$\mathbf{u} = \tilde{\mathbf{E}}_\omega\tilde{\mathbf{E}}_k(\omega)\mathbf{E}_k(\omega)(\boldsymbol{\Psi}_1(z)\boldsymbol{\psi}_1 + \boldsymbol{\Psi}_2(z)\boldsymbol{\psi}_2 + \boldsymbol{\Psi}_3(z)\boldsymbol{\psi}_3 + \boldsymbol{\Psi}_4(z)\boldsymbol{\psi}_4)e^{\mathrm{i}\omega t}, \tag{26}$$

where

$$\mathbf{\Psi}_1(z) = \mathrm{diag}[\mathrm{e}^{\mathrm{i}k_i(\omega)z}], \quad \mathbf{\Psi}_2(z) = \mathrm{diag}[\mathrm{e}^{-\mathrm{i}k_i(\omega)z}],$$

$$\mathbf{\Psi}_3(z) = \mathrm{diag}[\mathrm{e}^{-k_i(\omega)z}], \quad \mathbf{\Psi}_4(z) = \mathrm{diag}[\mathrm{e}^{k_i(\omega)z}]$$

and $\boldsymbol{\psi}_1$ to $\boldsymbol{\psi}_4$ are the modal coefficient vectors.

2.2.2. *Discretely supported multiple-mode model*

With the mounting of the rail on sleepers at discrete intervals in mind, the influence of the discrete support on higher vibration modes of a waveguide needs to be examined. For this reason, the solution of the multiple-mode model on a discrete support is derived in this section. Grassie *et al.* [6], among other authors, used the inter-element transfer matrix to calculate the direct receptance of infinitely long, discretely supported systems. The method applied here is based on this concept.

The system of Figure 3 consisting of $n = 3$ elastically connected beams can be divided into an infinite number of identical basic sections of length $L = L_1 + L_2$ consisting of two unsupported parts of length $L_1/2$ and a supported part of length L_2 between them as shown in Figure 4.

The dimensionless state vector at the beginning of the rth section on the right side of the excitation is defined as

$$\begin{aligned}\mathbf{v}_r &= \left[\frac{L^2}{EI_1}F_1, \ldots, \frac{L^2}{EI_n}F_n, \theta_1, \ldots, \theta_n, \frac{L}{EI_1}M_1, \ldots, \frac{L}{EI_n}M_n, \frac{1}{L}y_1, \ldots, \frac{1}{L}y_n\right] \\ &= \mathbf{S}[F_1, \ldots, F_n, \theta_1, \ldots, \theta_n, M_1, \ldots, M_n, y_1, \ldots, y_n], \end{aligned} \tag{27}$$

where y_i, θ_i, F_i, M_i are the displacement, the rotation, the shear force and moment at beam i for a model consisting of n beams.

A transfer matrix $\mathbf{T}$ is introduced which relates the state vector $\mathbf{v}_r$ at the beginning of the section r with the corresponding vector $\mathbf{v}_{(r+1)}$ of section $(r + 1)$ according to equation (28),

$$\mathbf{v}_{(r+1)} = \mathbf{T}\mathbf{v}_r. \tag{28}$$

The transfer matrix $\mathbf{T}$ is composed of the transfer matrices $\mathbf{C}$ and $\mathbf{D}$ of the unsupported and the supported subsections of the model respectively. Matrices $\mathbf{C}$ and $\mathbf{D}$ can be built up using the modal solution (26) by relating the state vectors at both sides of the subsections

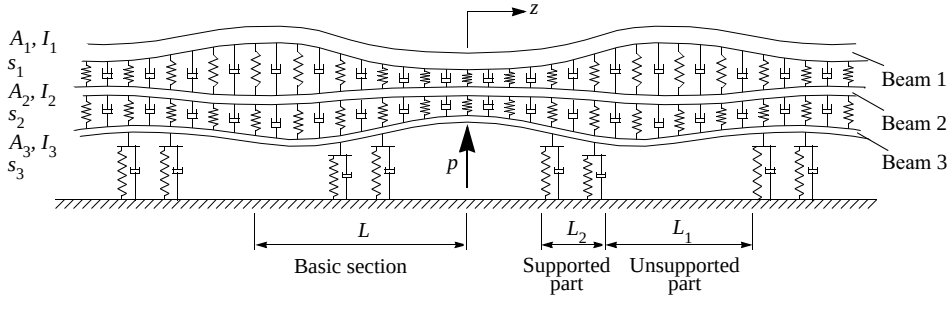

Figure 3. Multiple-mode model on discrete supports.

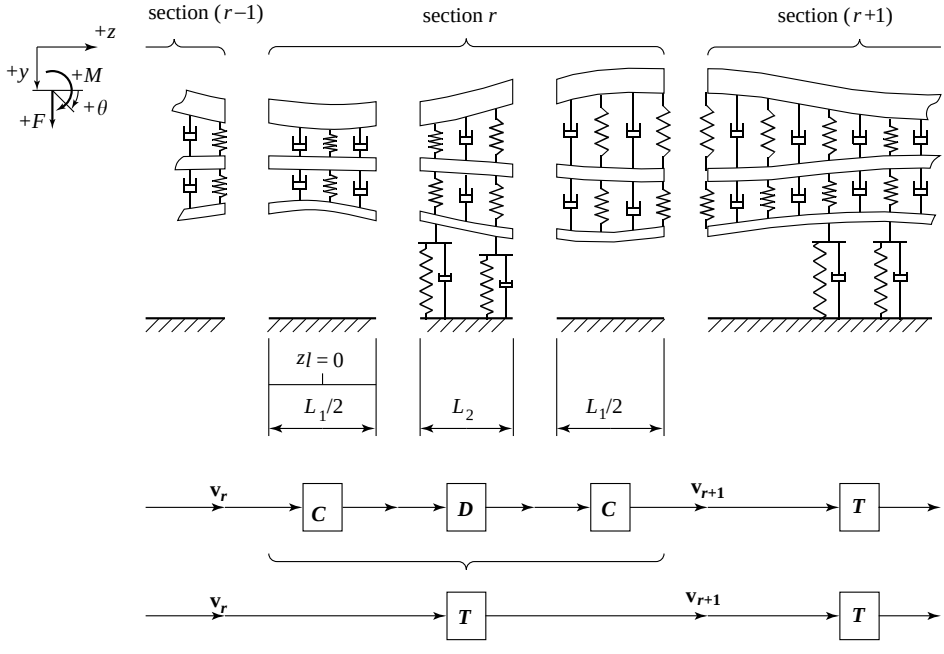

Figure 4. Basic section of discretely supported multiple-mode model and its transfer matrix representation.

and thus eliminating the modal coefficient vectors $\boldsymbol{\psi}_1$ to $\boldsymbol{\psi}_4$ (cf. Grassie *et al.* [6]). The eigenvalues of $\mathbf{T} = \mathbf{CDC}$ appear in inverse pairs $(q_i, 1/q_i)$, corresponding to left and right travelling waves respectively.

The relation

$$\mathbf{v}_0^{(2)} = \mathbf{H}\mathbf{v}_0^{(1)} \tag{29}$$

is found by eliminating eigenvalues with moduli greater than unity. Equation (29) relates the given values $\mathbf{v}_0^{(1)}$ (i.e., shear forces and beam rotations) and the unknown quantities $\mathbf{v}_0^{(2)}$ (i.e., displacements and moments) at the excitation point.

2.2.3. *Discussion of model*

The direct receptances of beam 1 of the continuously and discretely supported model are shown in Figure 5. The models are excited with a harmonic point force at beam 3. The parameters used in the calculation are chosen to give a realistic order of magnitude of the static deflection and of the lowest cut-off frequency compared with the rail studied experimentally (cf., Figure 9). The modal damping parameters of the continuously supported model are set to $\eta_i = 1/200$ and $\delta_i = 0$, giving Q^{BW}-factors of 200 for all modes. At the discretely supported model configuration, the modal damping of the unsupported parts ($s_3 = 0$) is set to $\eta_{u,i} = 1/800$ and the damping parameters of the supported areas $\eta_{s,i}$ are adjusted to achieve Q^{BW}-factors of 200 of the overall system as well. This damping distribution was chosen based on the expectation that system damping of a railway track occurs mainly at the sleepers.

The set of model parameters shown in Table 1 was chosen based on these considerations. It must be pointed out that the multiple-mode model is merely used to qualitatively study and understand the higher mode behavior of a waveguide, and is not intended to exactly reproduce the system response of an actual rail.

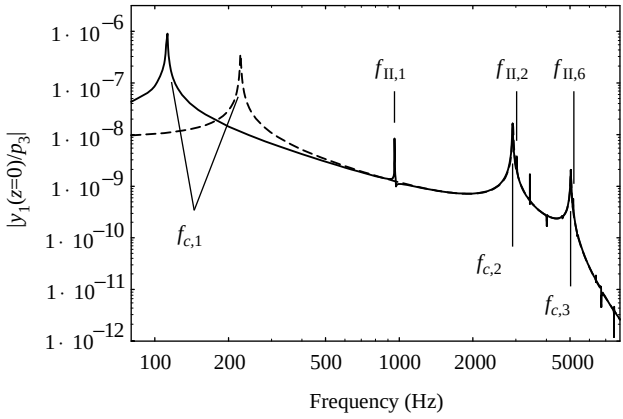

Figure 5. Direct receptance at beam 1 of continuously (— - —) and discretely (——) supported multiple-mode model with excitation force at beam 3.

TABLE 1

Parameter values of the unsupported, the continuously supported and the discretely supported model configuration

	Notation	Data	Notation	Data	Notation	Data
Flexural stiffness (Nm^2)	EI_1	1·2E6	EI_2	1·7E6	EI_3	0·5E6
Mass per unit length (Kgm^{-1})	ρA_1	15·0	ρA_2	15·0	ρA_3	15·0
Stiffness coefficient (Nm^{-2})	s_1	5·0E9	s_2	5·0E9		
Additional parameters of the continuously supported model configuration						
Stiffness coefficient (Nm^{-2})		—		—	s_3	9·0E7
Modal damping	η_1	5·0E3	η_2	5·0E3	η_3	5·0E3
Additional parameters of the discretely supported model configuration						
Length (m)	L	0·67	L_1	5·025E-1	L_2	1·675E1
Parameters of the unsupported model subsections						
Stiffness coefficient (Nm^{-2})		—		—	$s_{u,3}$	0·0
Modal damping	$\eta_{u,1}$	1·25E3	$\eta_{u,2}$	1·25E3	$\eta_{u,3}$	1·25E3
Parameters of the supported model subsections						
Stiffness coefficient (Nm^{-2})		—		—	$s_{s,3}$	9·0E7
Modal damping	$\eta_{s,1}$	5·0E3	$\eta_{s,2}$	1·62E2	$\eta_{s,3}$	1·12E2

The direct receptances shown in Figure 5 of both model configurations show prominent peaks at the cut-off frequencies $f_{c,i}$ of all three modes (type I resonances). Only the first cut-off frequencies $f_{c,1}$ of the continuously and discretely supported model differ noticeably. The value for the support stiffness presented in Table 1 was not adjusted so that the stiffness per unit length is not the same in the two models causing the different cut-off frequencies $f_{c,1}$. However, the cut-off frequencies $f_{c,2}$ and $f_{c,3}$ at approximately 2910 and 5030 Hz, respectively, are barely influenced by the type or the stiffness of the support. Additional amplitude maxima are observed in the discretely supported case, for example at $f_{II,1} = 957$ Hz, $f_{II,2} = 3024$ Hz and $f_{II,6} = 5148$ Hz. In the studied numerical example, the frequencies $f_{II,2}$ and $f_{II,6}$ are slightly higher than $f_{c,2}$ and $f_{c,3}$, respectively. There are three additional amplitude peaks of the discretely supported model between the frequencies

TABLE 2

Cut-off frequencies of the unsupported ($f_{c,A}$), the continuously supported ($f_{c,B}$) and the discretely supported model configuration ($f_{c,C}$ and $f_{\mathrm{II},(1,2,6)}$) and their relative deviations

Mode	$f_{c,C}$ (kHz)	$f_{c,B}$ (kHz)	$2(f_{c,C}-f_{c,B})/(f_{c,C}+f_{c,B})$ (%)	$f_{c,A}$ (kHz)	$2(f_{c,C}-f_{c,A})/(f_{c,C}+f_{c,A})$ (%)	$f_{\mathrm{II},(1,2,6)}$ (kHz)	$2(f_{c,C}-f_{\mathrm{II}})/(f_{c,C}+f_{\mathrm{II}})$ (%)
1	0·112	0·224	66·556	0·000	—	0·957	158·047
2	2·909	2·919	0·339	2·906	0·111	3·024	3·887
3	5·033	5·035	0·045	5·033	0·005	5·148	2·261

$f_{\mathrm{II},2}$ and $f_{\mathrm{II},6}$ which are not considered in further detail. All of these peaks are caused by resonance effects of the periodic system and are called type II resonances throughout this work. The first type II resonance at 957 Hz corresponds to the pinned–pinned frequency often referred to in the literature. The system at the higher type II frequencies shows a periodic motion according to the sleeper spacing with a cross-sectional deformation similar to one of the mode shapes at its cut-off frequency. More details regarding this phenomenon are given in the discussion of Figure 6 later in this section.

The exact frequencies of the amplitude maxima are summarized in Table 2. The cut-off frequencies of the continuous model without support ($s_3 = 0$) are included. Table 2 also contains the relative deviations between the frequencies. Table 2 confirms that the cut-off frequencies of higher modes are barely influenced by the presence or the type of the support in the presented numerical example, where the stiffness of the support is small compared with the stiffness of the connecting layers. With the rail mounted on sleepers and ballast in mind, this assumption seems reasonable and is confirmed by the experiments presented in section 4. The presented example also shows that depending on support parameters such as sleeper spacing, the frequencies of type II resonances of the discretely supported model can be close to the cut-off frequencies of the waveguide.

Figure 6 shows the beam displacements of the discretely supported model at the cut-off frequency $f_{c,2}$ and at type II resonance frequency $f_{\mathrm{II},2}$ which is adjacent. Hatched areas beneath the displacement curve of beam 3 identify supported regions of the discretely supported model.

The mode shape of mode 2 for both the discretely and the continuously supported model is characterized by a 180° out-of-phase movement of beams 1 and 3 and a small amplitude at beam 2. This is observed at both presented frequencies of the discretely supported model. However, the spatial behavior is completely different. The type II response at $f_{\mathrm{II},2}$ shows no localized vibration zone close to the excitation. The amplitude of the system response decreases at the supported areas of the model and builds up again in the unsupported regions. At the cut-off frequency $f_{c,2}$, a vibration zone of approximately 4–6 sleeper spacings in extent is observed. Beyond this region, a wave is travelling with comparably small amplitude. This type of system response showing a localized vibration zone close to the excitation and a propagating wave further away is later referred to as the typical cut-off frequency behavior or type I response.

At a given excitation frequency, different modes contribute to the total displacement of the propagating waves with various degrees. This effect has been pointed out by Wu and Thompson [8] and can be shown by plotting the actual contribution of each mode to the beam displacement with increasing distance from the excitation. In Figure 7, the modal contributions to the displacement of beam 1 is shown in the example of the continuously

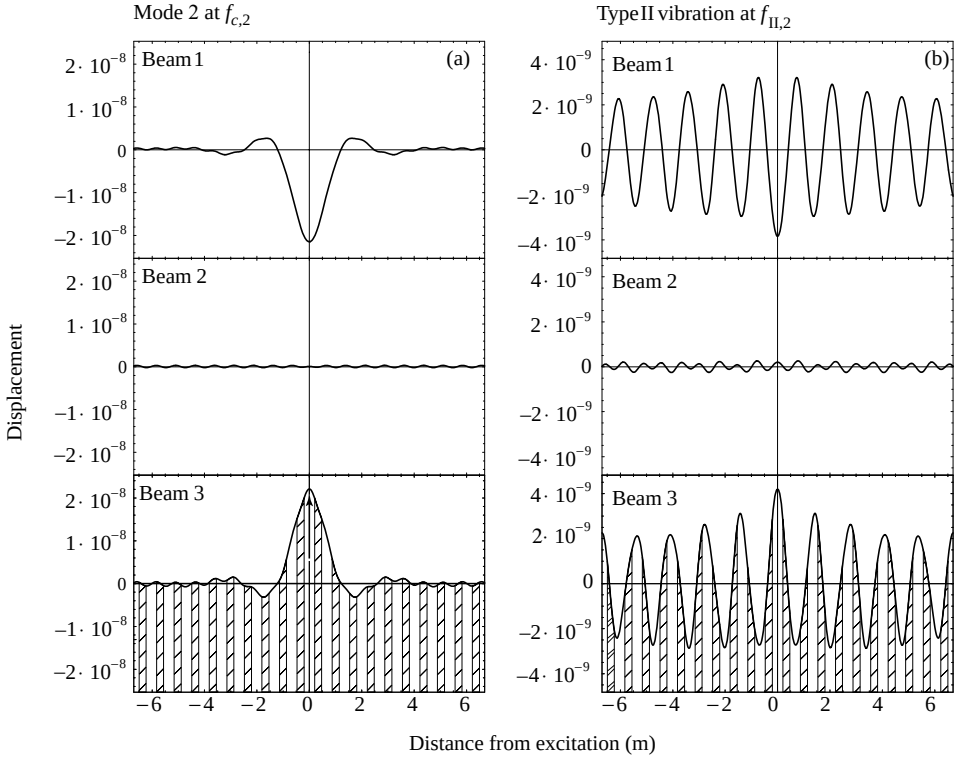

Figure 6. Beam displacements of the discretely supported multiple-mode model at the cut-off frequency $f_{c,2} = 2910$ Hz (a) and at the frequency $f_{II,2} = 3020$ Hz (b).

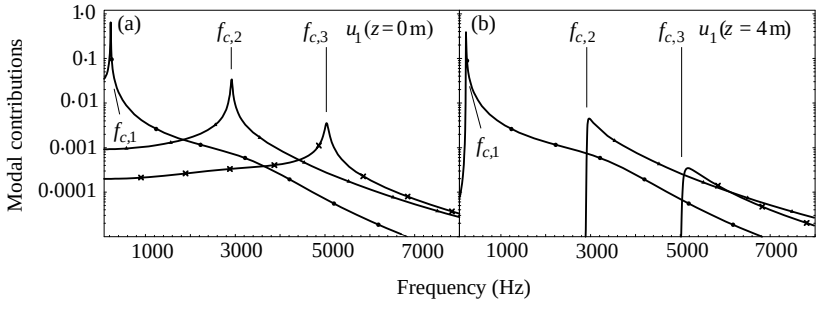

Figure 7. Contributions of each mode to the displacement of beam 1 of the continuously supported multiple-mode model at $z = 0$ (a) and $z = 4$ m (b) for modes: –●–, 1; –▲–, 2; –×–, 3.

supported model. If the system is excited with the cut-off frequency of a certain mode, the displacement at the point of excitation is dominated by the mode shape of the respective mode. The situation at some distance from the excitation has changed for higher modes. The spatial decaying rate of the mode which is excited at its cut-off frequency is high compared with lower modes. This means that travelling waves of lower modes become more and more important with increasing distance from the excitation.

With an excitation at the cut-off frequency of a certain mode, these observations imply that the behavior of the respective mode dominates the system response in the vicinity of the excitation. This justifies the use of Bernoulli–Euler beams instead of Timoshenko beams in

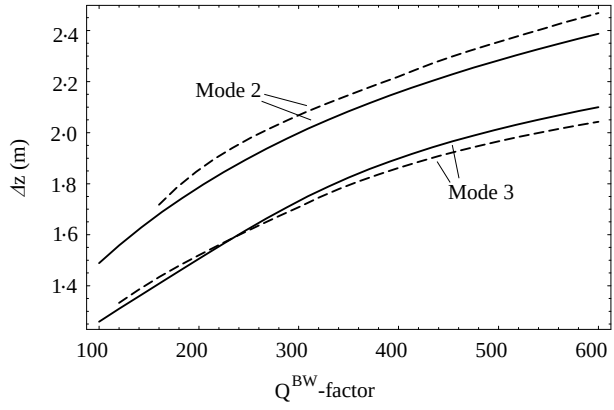

Figure 8. Relation between Q^{BW}-factor and the size of the vibration zone Δz with continuous (——) and discrete (– · –) support.

the multiple-mode model, since the localized vibration zone close to the excitation is of major importance for the examined application of train wheel detection.

The region of large vibration amplitude according to the mode shape of the excited mode was called the localized vibration zone while discussing Figure 6. Let the quantity Δz be defined as

$$|y_i(z = \Delta z/2)| = |(y_i(z = 0)|\mathrm{e}^{-1} \tag{30}$$

to quantitatively describe the size of the localized vibration zone.

Figure 8 shows the relation between the Q^{BW}-factor and the size of the localized vibration zone Δz for modes 2 and 3 of the continuously and the discretely supported multiple-mode model. This illustrates that the localized vibration zone decreases with increasing damping and with increasing frequency. The type of the support, continuous or discrete, has a comparably small influence.

3. NUMERICAL CALCULATION OF CUT-OFF FREQUENCIES AND MODE SHAPES

Assuming that a linear theory of wave motion is applicable, and taking the z-direction as the direction of propagation, plane waves with angular frequency ω and wavenumber k of the form

$$\mathbf{u}(x, y, z, t) = \mathrm{e}^{\mathrm{i}(kz + \omega t)}\mathbf{u}(x, y) \tag{31}$$

are sought, where $\mathbf{u}(x, y, z, t)$ is the displacement vector of the rod. Rosenfeld and Keller [10] studied waves of this type in rods of arbitrary cross-section. They obtained asymptotic expansions of the exact solutions for both small and large values of the dimensionless wavenumber (ka), where a is a typical dimension of the cross-section. In addition to four modes propagating at low frequencies, also referred to as the lowest longitudinal, torsional and flexural modes, there are infinitely many other modes. These modes are referred to as higher modes throughout this paper. Each of them has a cut-off frequency $\omega_{c,i}$ below which it cannot propagate. At the cut-off frequency, the wavenumber is zero and the wavelength tends to infinity in the absence of damping and supports. To analyze these higher modes near their cut-off frequencies, Rosenfeld and Keller [10] expanded the displacement vector $\mathbf{u}(x, y)$ and the phase velocity in powers of (ka). By using these expansions in the equations of

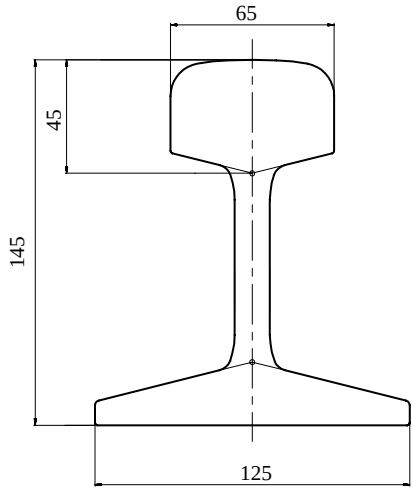

Figure 9. Cross-section of studied rail type SBB I. Dimensions given in mm.

TABLE 3

Experimentally determined cut-off frequencies of symmetric modes and asymmetric modes. Observed spatial behavior according to type I *behavior with vibration zone* Δz (†), *type II vibration* (‡) *or a combination of both response types* (§)

Mode	Calculated (kHz)	Measured (kHz)	Relative deviation (%)	Δz (m)
Symmetric modes				
6	6·24	6·20‡	0·6	—
7	11·57	11·58‡	0·1	—
10	24·19	24·11§	0·3	—
12	26·69	27·64	3·6	—
13	32·52	31·69‡	2·6	—
15	36·12	36·17‡	0·1	—
18	42·61	42·69†	0·2	0·2
20	49·82	49·20†	1·2	0·1
Asymmetric modes				
8	11·62	11·42†	1·7	0·4
9	17·12	16·98†	0·8	0·4
11	25·19	24·94†	1·0	0·3
14	35·70	35·77§	0·2	—
16	39·75	—	—	—
17	41·35	41·47†	0·3	0·25
19	44·67	45·06†	0·9	0·5

motion and in the boundary condition, they obtained equations for the coefficients in the expansions. The modes were found to be of two types. The first type shows a mainly longitudinal displacement.

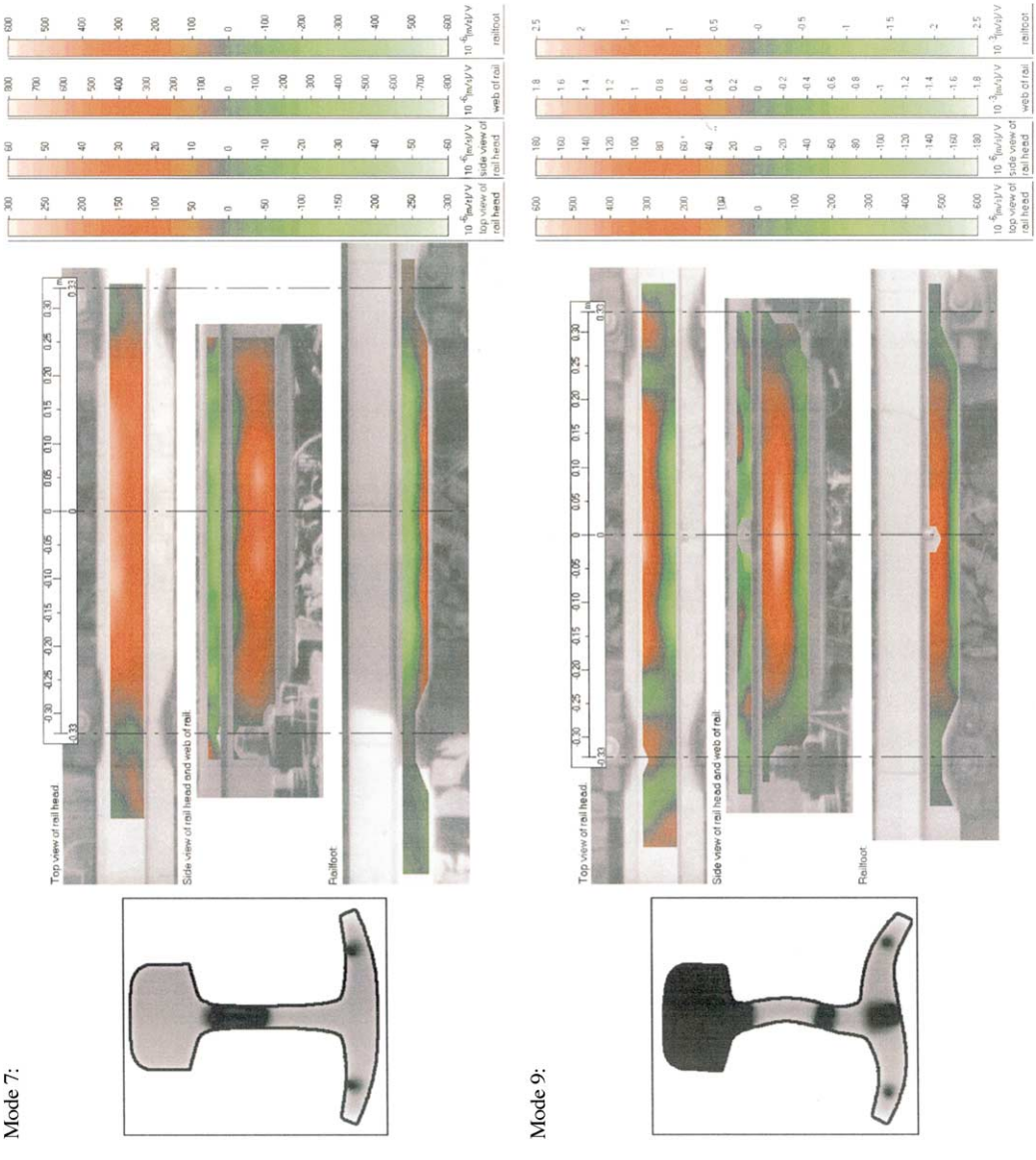

Figure 10. Numerically calculated mode shape of the cross-section (boxed pictures; dark corresponds to no motion) and measured mode shape between two sleepers at cut-off frequency of mode 7 (foot excitation, graphs on the left side of figure) and mode 9 (head excitation, graphs on the right side of figure) with excitation at $z = 0$ m. The following views are shown: top view of rail head, side view of rail head and web of rail and top view of railfoot. The scaling of the measured mode shapes is given on the right side.

For the second type the displacement is primarily transverse. There are infinitely many modes of each type. Their cut-off frequencies are the eigenvalues of two different eigenvalue problems associated with the cross-section. Because of experimental considerations regarding both excitation and measurement, only transverse modes are considered here, corresponding to the eigenvalue problem of the cross-section subjected to plane strain.

All experiments presented in Section 4 were carried out at a track with rails of the Swiss-type *SBB* I. The geometry of this rail type is shown in Figure 9.

The higher vibration modes of this cross-section, if subjected to plane strain, were calculated using a standard finite element code (SDRC I-DEAS).

Counting the torsional and the two flexural modes which exist at low frequencies as discussed above as the first three modes with transverse motion, the first higher transverse vibration mode is called mode 4. Although not explicitly referred to throughout the rest of this paper, all discussed vibration modes are transverse modes. Mode 4 with a cut-off frequency of 1·46 kHz and mode 5 with a cut-off frequency of 4·26 kHz are for experimental reasons not examined any further, leaving a total of 15 higher modes of the studied rail type in the defined frequency range from 5 to 50 kHz. The numerically calculated cut-off frequencies are listed in Table 3 and some typical mode shapes are depicted in Figure 10. These results are discussed later with the experiments.

4. EXPERIMENTS

4.1. FREQUENCY SPECTRA AND MODE SHAPE MEASUREMENTS

The frequency spectrum and the mode shapes of the rail according to Figure 9 at their cut-off frequencies were experimentally examined in the frequency range from 5 to 50 kHz. The studied test track was mounted on wooden sleepers and ballast. A scanning vibrometer based on a heterodyne laser interferometer was used to measure the velocity at the surface of the rail. The laser beam is deflected using two built-in mirrors, thus allowing the vibration measurement at each point of a defined grid. The mode shapes are calculated from the recorded data at user-defined bands by performing a standard modal analysis based on the fast Fourier transform (FFT).

Measurements of the mode shapes on top of the rail head, at the side of the rail head, at the web of the rail and on top of the railfoot were performed. Figure 11 shows the measurement grid used.

A periodic chirp signal was used to excite the rail. The total frequency range was divided into intervals of 0–20, 20–30, 30–40 and 40–50 kHz in order to have sufficient signal energy at each interval. Piezoelectric transducers with a small backing mass mounted at the center of the railfoot beneath the rail and at the side of the rail head were used to excite symmetric and asymmetric modes, respectively. Figure 12 illustrates the positions of the transducers. The receiving transducers shown in Figure 12 are used for the damping measurements discussed in section 4.2. Acting as high-pass filters, the transducers produce a sufficient excitation amplitude only when measuring at more then approximately 5 kHz.

The dynamic response of a rail measured at a single point shows a high degree of complexity at frequencies above approximately 2 kHz (cf. reference [11]). However, the amplitude maxima at the cut-off frequencies can be made more visible by calculating the average spectrum of several measurement points close to the excitation. Figure 13 shows the average spectrum of the transfer function β between the voltage of the excitation signal and the velocity measured at all points of the grid shown in Figure 11.

By looking at the mode shapes at frequency bands around the peaks in the averaged spectra close to the numerically predicted cut-off frequencies, the modes could be matched with the calculated ones (Figure 13). Except for mode 16, all calculated higher modes in the frequency range from 5 to 50 kHz could be located. The measured and the numerically calculated mode shapes of modes 7 and 9 are presented in Figure 10. Additional observed peaks are attributed to longitudinal modes or to the discrete supports.

Mode 7 is characterized by a vertical movement of the rail head and a symmetric flapping vibration of the railfoot. The web of the rail at mode 9 is subjected to bending with a node at the lower third of its height. Compared with mode 7, the node at the railfoot is closer to the end. The head of the rail performs a rotating movement with a vibration node at the middle

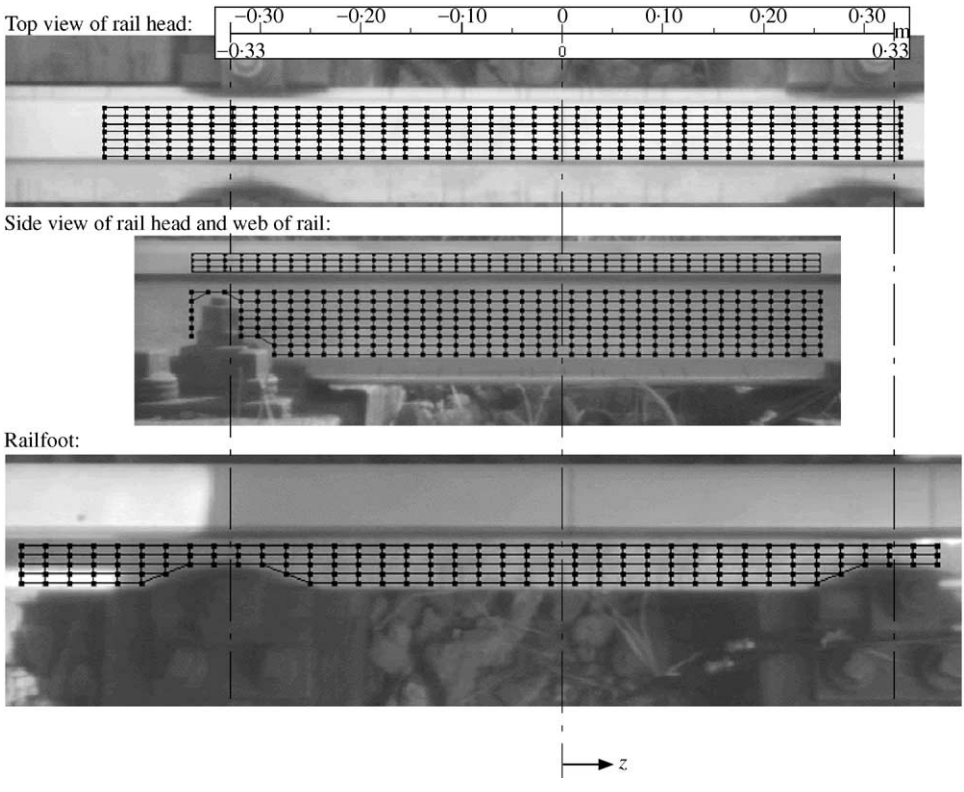

Figure 11. Measurement grid used: top view of rail head (top picture), side view of rail head and web of the rail (middle picture) and top view of railfoot (bottom picture). Excitation at $z = 0$ m.

of the running surface. Although the amplitude of this rotation is comparably small, it is clearly visible in the measurement.

The behavior of these two modes along the rail direction is shown in Figure 14. The vibration on top of the rail head of three adjoining rail–sleeper sections have been recorded and connected to give a continuous picture.

The vibration of the rail head at mode 7 decreases at the sleepers and builds up again in the following free section of the rail. This behavior corresponds to type II response observed at the discretely supported multiple-mode model. It can be seen from the value ranges of each of the three subsections that the overall spatial decay is modest at this mode.

Mode 9 shows a vibration zone of less than one sleeper spacing at the excitation. Beyond this region a travelling wave can be observed. The amplitude at the vibration zone is approximately four times larger compared with the wave which can be observed by looking at the value ranges. The amplitude of the travelling wave at the second and the third span stays more or less unchanged. This type of system response corresponds to the typical cut-off frequency behavior (type I behavior) predicted by the multiple-mode model.

The calculated and experimentally determined cut-off frequencies and their relative deviations are summarized in Table 3. The table also contains a classification of the modes according to their spatial behavior. The size of the vibration zone Δz is included for modes which show type I response.

The calculated and experimentally determined cut-off frequencies agree within 4% and more often even better than within 1%. This confirms the statement derived from the multiple-mode model that the type of support has a marginal influence on the cut-off

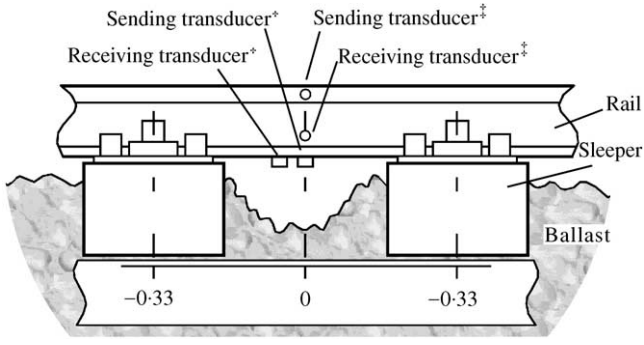

Figure 12. Positions of sending and receiving transducers used for excitation of symmetric modes (†) and of asymmetric modes (‡).

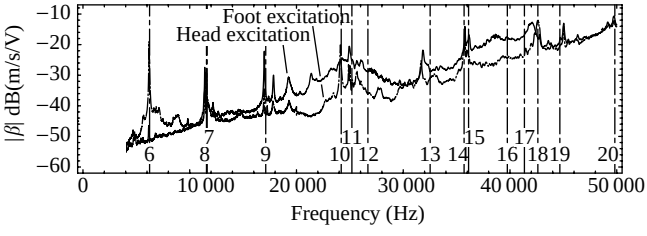

Figure 13. Average spectrum of transfer function β between the voltage of the excitation signal and the velocity over all points of measurement grid (approximately 900 pts) with foot excitation and head excitation. Calculated cut-off frequencies are marked by numbers and | lines.

frequencies of higher vibration modes. The missing of the asymmetric mode 16 can be explained by the unfavorable position of the exciting transducer, as the motion of the rail head has a small amplitude in a mainly vertical direction for this mode. Seven modes show the typical cut-off frequency behavior with a localized vibration zone close to the excitation, and a travelling wave occurring beyond this region. Type II behavior with a vibration according to the corresponding mode shape which builds up at the free rail segments between the sleepers is observed at four modes. All of these modes are symmetric modes. Two modes show a combination of both effects with a vibration at the first and the second span with an overlaying wave. No clear classification was possible at mode 12 due to a small amplitude at the rail head.

The size of the localized vibration zone Δz of the modes with type I response varies between approximately 0·1 and 0·5 m. Except for mode 19, a decreasing tendency of the vibration zone Δz is observed with increasing frequency. This is in agreement with the predictions made by the multiple-mode model.

4.2. DAMPING MEASUREMENT

The quality factors of several modes have been determined by measuring the transfer function $\beta_e(f)$ from the sending to the receiving transducer at the corresponding cut-off frequencies (see Figure 12). The magnitude and phase response have been recorded using a lock-in amplifier by changing in a stepwise manner the excitation frequency close to the cut-off frequencies. A least-squares fit of the experimental data was performed in order to

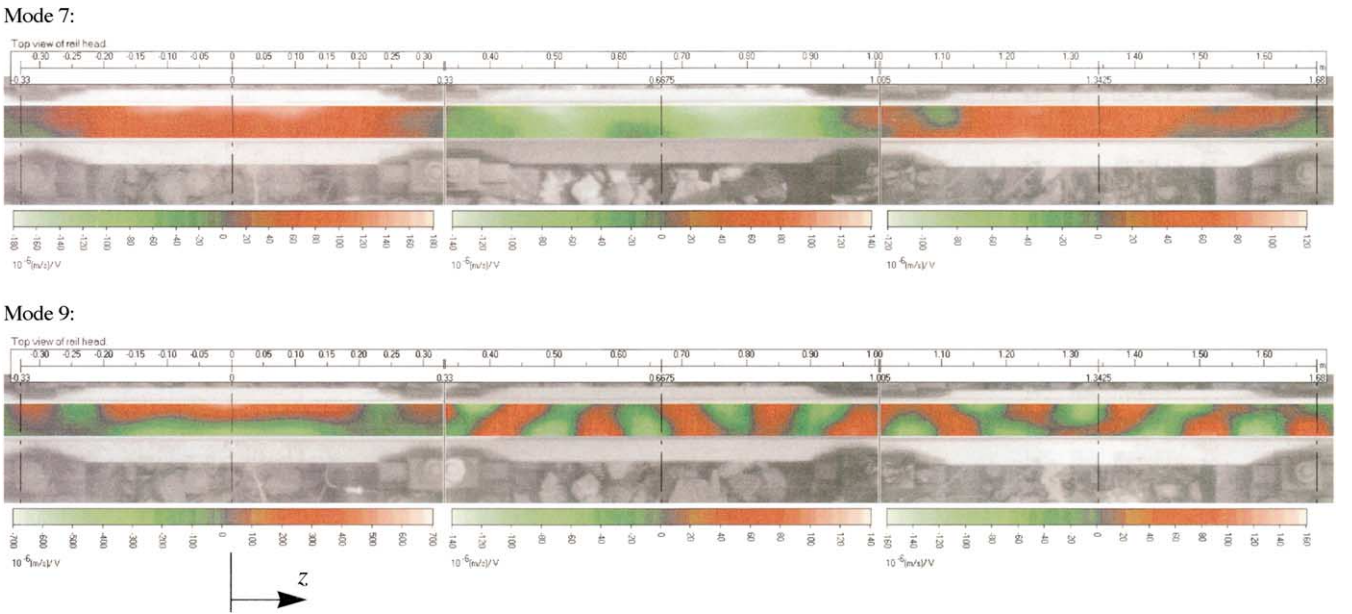

Figure 14. Spatial behavior of modes 7 and 9 measured at the running surface over a distance of three sleeper spacings from the excitation at $z = 0$ m.

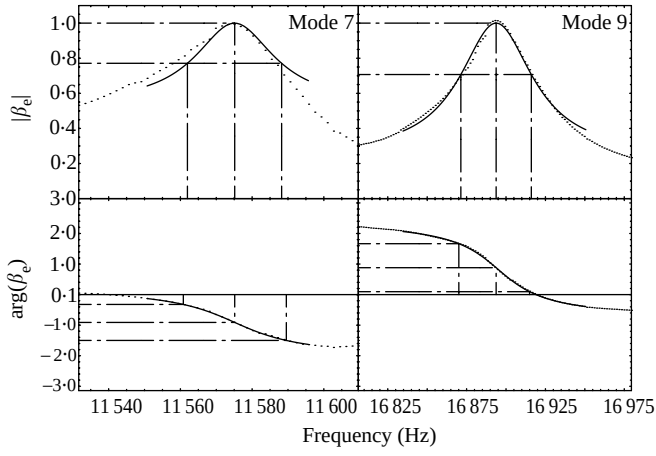

Figure 15. Normalized magnitude and phase response of modes 7 and 9. Fitted curves used to determine the quality factors are included.

estimate the parameters f_c and a_1 to a_6 of the approximation functions (32) and (33):

$$|\beta_e(f)|_{\text{fit}} = a_1/((f_c^2 - f^2)^2 + a_2) + a_3, \tag{32}$$

$$\arg(\beta_e(f))_{\text{fit}} = a_4 \arctan(\, a_5/(f_c^2 - f^2)) + a_6. \tag{33}$$

Figure 15 shows the normalized magnitude and phase response of modes 7 and 9 including the approximation functions.

The total phase change of mode 7 is close to $3\pi/4$. This corresponds to the phase change of a beam on a viscoelastic foundation as studied in section 2.1. The magnitude response of mode 7 differs from an ideal response behavior, most specifically in regard to its symmetry.

An observed total phase change close to 180° at mode 9 corresponds to the behavior of a s.d.o.f. mechanical oscillator.

Using the approximation functions, the quality factors Q and Q^{BW} of six selected modes have been determined by finding the frequencies where the magnitude and phase have changed by $1/\sqrt{2}$ and $\pm\pi/4$ or by $1/\sqrt[8]{8}$ and $\pm 3\pi/16$ compared with the values at the cut-off frequency. The classical Q-factor method was applied to modes which showed a total phase change $\Delta\varphi$ of approximately π; the Q^{BW}-factor was used for modes with phase changes close to $3\pi/4$. The quality factors obtained along with the observed total phase changes $\Delta\varphi$ are summarized in Table 4. The resulting time constants $t_{1/e}$ are also included in the table.

Three of the studied modes show a total phase change $\Delta\varphi$ between 170° and 180° which can be regarded as classical resonance behavior. The Q-factor was determined for these modes and evidenced values from the magnitude and the phase measurement which were compatible within 4%.

The second group of modes has a total phase change $\Delta\varphi$ between 135 and 155°. The Q^{BW}-factor is more appropriate for characterizing the damping of these modes, and gives quality factors from the magnitude and the phase measurement which were within approximately 5% compatible. Applying the Q-factor method to these modes with phase changes close to 135°gives quality factors from magnitude and phase measurement differing approximately 20–40%. The Q-factor values would be approximately 30% lower than the obtained Q^{BW}-factors. This is caused by the fact that the Q-factor does not take into account the fact that energy travels away from the excitation due to wave propagation.

TABLE 4

Quality factors from magnitude and phase of measured transfer functions and the resulting reaction times $t_{1/e}$

Mode	f_c (kHz)	$\Delta\varphi$ (°)	Quality factor from		Relative deviation (%)	$t_{1/e}$ (10^{-3} s)
			Magnitude	Phase		
6	6·20	189	155·1†	156·3†	0·8	8·0
7	11·57	136	421·5‡	403·0‡	4·5	11·3
8	11·31	171	256·6†	247·3†	3·7	7·1
9	16·89	186	377·9†	376·5†	0·4	7·1
10	24·13	153	505·5‡	531·8‡	5·1	6·8
18	42·58	142	193·5‡	192·4‡	0·6	1·4

†Q-factor method used for modes with phase changes $\Delta\varphi$ close to 180°.
‡Q^{BW}-factor used for modes with phase changes $\Delta\varphi$ close to 135°.

The time constants $t_{1/e}$ of the mechanical system obtained from the Q-factors and Q^{BW}-factors are of the order of a few milliseconds with a decreasing tendency towards higher frequencies. The time constant corresponds to the reaction time of the sensor. A train wheel travelling at a velocity of 150 km/h needs 9·6 ms to pass a local vibration zone of 0·4 m in extent. This passing time is close to the time constants found, and means that measures must be taken in order to ensure a reliable axle detection. The time constant of the mechanical system could be improved by adding additional damping at the localized vibration zone.

The presented damping measurements also raise some open questions which are discussed in the following section.

The multiple-mode model gave phase changes of the receptance of less than $\pi/4$ for type II resonances caused by the discrete support. Although some of the experimentally investigated modes show the typical spatial behavior of these type II resonances, no total phase changes of less then $3\pi/4$ have been found. No clear connection between the spatial behavior of the modes and the observed total phase change could be found. Modes 8 and 9, which showed the typical type I behavior, have phase changes close to 180° instead of 135° as would be expected. The total phase change of mode 6 showing type II spatial behavior is 180° and mode 7, also with type II behavior, has a total phase change of 135°. The reason why the observed range of phase changes is limited by 135° and 180° is currently not understood and further investigation is needed, with a possible explanation being a superposition of type I and type II behavior resulting from the high density of type II resonance frequencies.

5. CONCLUSIONS

The forced vibration response of a railway track which is excited at its higher cut-off frequencies has been examined theoretically, numerically and experimentally.

The behavior of higher modes at their cut-off frequencies in a waveguide has been studied using a model consisting of several elastically connected beams including modal damping. It has been shown that a local vibration zone near the excitation exists in the presence of system damping. The size of this vibration zone is controlled by damping and frequency. The intention is to use this vibration zone within a sensing device to detect passing train wheels. Additional resonance effects originating from the periodic support exist and are

referred to as type II vibrations. Depending on support parameters such as sleeper spacing, these type II resonance frequencies can occur close to the cut-off frequencies of the waveguide. In this case, the cross-sectional mode shape close to the excitation of type II vibration is similar to the mode shape at the corresponding cut-off frequency. However, type II vibrations show no localized vibration zone and are therefore not suitable for single-wheel detection.

The cut-off frequencies and mode shapes of the rail type at which the experiments were carried out have been numerically predicted by solving the eigenvalue problem of the rail cross-section subjected to plane strain. It was possible to measure 14 of 15 higher vibration modes in the frequency range from 5 to 50 kHz. The experiments showed that the calculated and measured cut-off frequencies and mode shapes correspond well, close to the excitation. The typical cut-off frequency behavior with a local vibration zone close to the excitation has been observed for the majority of the measured modes. Some modes, however, showed a vibration according to the respective mode shape building up between several neighboring sleepers and small amplitudes at the sleepers. This corresponds to type II vibration behavior. The observed overall spatial decay of these vibrations is modest, and is as such in agreement with the model predictions.

The damping of several modes has been determined by measuring the quality factors from the amplitude and the phase response of the rail. Two types of responses have been experimentally observed. A first group of modes showed a total phase change of close to π and a second group showed phase changes close to $3\pi/4$. Motivated by the analytical model of a beam on a viscoelastic foundation, an adopted measurement method referred to as Q^{BW}-factor has been applied to the latter group of modes. No clear connection between the spatial behavior of the modes and their phase response could be established.

The following consequences can be drawn regarding the technical application of local rail vibrations.

It is possible to experimentally find and stabilize specific rail modes. However, due to the high density of amplitude peaks observed at a single measurement point, it is necessary to have multiple receiver signals in order to be able to distinguish between different vibration modes. These transducers would be mounted advantageously at several positions along the rail contour in order to find the characteristic motion of a certain vibration mode. Modes which show a type II response with no local vibration zone are not suitable for the detection of single train wheels. These modes can be excluded by mounting an additional receiver at the rail span next to the excitation.

The reaction times resulting from the damping measurement are close to the time which a wheel of a fast travelling train needs to pass the local vibration zone. In order to ensure a reliable wheel detection, the mechanical time constant of the rail vibration could be improved by adding extra damping to the local vibration zone.

ACKNOWLEDGMENTS

The authors wish to acknowledge the support given to this project by the Commission for Technology and Innovation KTI and the company Schweizer Electronic AG, both located in Switzerland.

REFERENCES

1. B. RIPKE and K. KNOTHE 1991 *VDI Fortschritt-Bericht*, Reihe 11, Nr. 155. Die unendlich lange Schiene auf diskreten Schwellen bei harmonischer Einzellasterregung.

2. W. SCHOLL 1987 *VDI Fortschritt-Bericht*, Reihe 11, Nr. 93. Darstellung des Körperschalls in Platten durch Übertragungsmatrizen und Anwendung auf die Berechnung der Schwingungsformen von Eisenbahnschienen.
3. D. J. THOMPSON 1991 *Proceedings of the Institution of Mechanical Engineers, Journal of Rail and Rapid Transit* **205F**, 137–149. Theoretical modelling of wheel–rail noise generation.
4. Z. STRZYZAKOWSKI and L. ZIEMANSKI 1991 *Zeitschrift für Angewandte Mathematik und Mechanik* **71**, 221–224. On the application of the finite strips method to dynamical analysis of vehicle-track system.
5. K. KNOTHE, Z. STRZYZAKOWSKI and K. WILLNER 1994 *Journal of Sound and Vibration* **169**, 111–123. Rail vibrations in the high frequency range.
6. S. L. GRASSIE, R. W. GREGORY, D. HARRISON and K. L. JOHNSON 1982 *Journal of Mechanical Engineering Science* **24**, 77–90. The dynamic response of railway track to high frequency vertical excitation.
7. T. X. WU and D. J. THOMPSON 1999 *Journal of Sound and Vibration* **224**, 329–348. A double Timoshenko beam model for vertical vibration analysis of railway track at high frequencies.
8. T. X. WU and D. J. THOMPSON 1999 *Journal of the Acoustical Society of America* **106**, 1369–1376. Analysis of lateral vibration behavior of railway track at high frequencies using a continuously supported multiple beam model.
9. M. R. PFAFFINGER 2000 *Ph.D. Thesis, Swiss Federal Institute of Technology Zurich*. Higher vibration modes in railway tracks at their cut-off frequencies.
10. G. ROSENFELD and J. B. KELLER 1974 *Journal of the Acoustical Society of America* **55**, 555–561. Wave propagation in elastic rods of arbitrary cross section.
11. N. VINCENT and D. J. THOMPSON 1995 *Vehicle System Dynamics* Supplement **24**, 100–114. Track dynamic behaviour at high frequencies. Part 2: experimental results and comparisons with theory.